

# Large Anisotropy Barrier in a Tetranuclear Single-Molecule Magnet Featuring Low-Coordinate Cobalt Centers

Khetpakorn Chakarawet,<sup>†</sup> Philip C. Bunting,<sup>†</sup> and Jeffrey R. Long<sup>\*,†,‡,§</sup>

<sup>†</sup>Department of Chemistry and <sup>‡</sup>Department of Chemical and Biomolecular Engineering, University of California Berkeley, Berkeley, California 94720, United States

<sup>§</sup>Materials Sciences Division, Lawrence Berkeley National Laboratory, Berkeley, California 94720, United States

**S** Supporting Information

**ABSTRACT:** The tetranuclear cobalt cluster compound  $[\text{Co}_4(\mu\text{-NP}^t\text{Bu}_3)_4][\text{B}(\text{C}_6\text{F}_5)_4]$  ( $^t\text{Bu}$  = *tert*-butyl) was synthesized by chemical oxidation of  $\text{Co}_4(\text{NP}^t\text{Bu}_3)_4$  with  $[\text{FeCp}_2][\text{B}(\text{C}_6\text{F}_5)_4]$  and magnetically characterized to study the effect of electronic communication between low-coordinate metal centers on slow magnetic relaxation in a transition metal cluster. The dc magnetic susceptibility data reveal that the complex exhibits a well-isolated  $S = 9/2$  ground state, which persists even to 300 K and is attributed to the existence of direct metal–metal orbital overlap. The ac magnetic susceptibility data further reveals that the complex exhibits slow magnetic relaxation in the absence of an applied field, and that the relaxation dynamics can be fit with a combination of Orbach, quantum tunneling, and Raman relaxation processes. The effective spin reversal barrier for this molecule is  $87\text{ cm}^{-1}$ , the largest reported to date for a transition metal cluster, and arises due to the presence of a large easy-axis magnetic anisotropy. The complex additionally exhibits waist-restricted magnetic hysteresis and magnetic blocking below 3.6 K. Taken together, these results indicate that coupling of low-coordinate metal centers is a promising strategy to enhance magnetic anisotropy and slow magnetic relaxation in transition metal cluster compounds.

More than two decades ago, the dodecanuclear Mn cluster  $\text{Mn}_{12}\text{O}_{12}(\text{O}_2\text{CCH}_3)_{16}(\text{H}_2\text{O})_4$  was shown to exhibit a bistable magnetic ground state separated by an energy barrier to spin relaxation,  $U$ .<sup>1</sup> It was found that when the thermal energy is small compared to  $U$ , the molecule can retain its magnetization for months at a time and also exhibits magnetic hysteresis, a phenomenon previously thought to be relegated to bulk magnetic materials. This seminal discovery launched the field of single-molecule magnetism. Due to their nanometer size and unique tunability, these molecular magnets have been touted as promising candidates for applications in high-density data storage,<sup>2</sup> quantum information processing,<sup>3</sup> and spintronics.<sup>4</sup> Yet, the majority of single-molecule magnets exhibit relaxation barriers well below 300 K, while their practical operating temperatures, i.e., those temperatures at which the magnetization retains its orientation, are even lower (tens of K at most).<sup>5</sup>

In pursuit of potential applications and the requisite longer relaxation times at higher temperatures, much focus in molecular magnetism research has been invested toward increasing the spin

reversal barrier,  $U$ . For transition metal-based single-molecule magnets, this barrier is formulated as  $U = |D|S^2$  (for integer spin systems) or  $U = |D|(S^2 - 1/4)$  (for half-integer spin systems), where  $S$  is total electron spin and  $D$  is axial zero-field splitting parameter (with its sign and magnitude corresponding to the size and nature of the magnetic anisotropy).<sup>6</sup> The quadratic dependence of  $U$  on  $S$  motivated initial investigation into exchange-coupled transition metal clusters with large total spin. However, theoretical studies later showed that the anisotropy term  $D$  is inversely proportional to  $S^2$ , rendering  $U$  virtually invariant to  $S$ .<sup>7</sup> The current record for the largest spin reversal barrier exhibited by a transition metal cluster is  $60\text{ cm}^{-1}$ , a claim that has been held for over a decade by the  $S = 12$  complex  $\text{Mn}_6\text{O}_2(\text{Et-sao})_6(\text{O}_2\text{CR})_2(\text{EtOH})_6$  ( $\text{Et-saoH}_2 = 2$ -hydroxyphenylpropanone oxime;  $\text{R} = 3,5$ -dimethylphenyl).<sup>8</sup>

Alternatively, research on mononuclear transition metal single-molecule magnets has achieved significant progress toward enhancing magnetic anisotropy. Indeed, recently a mononuclear two-coordinate cobalt imido complex was shown to exhibit slow magnetic relaxation with a record barrier of  $413\text{ cm}^{-1}$ .<sup>9</sup> Even still, a continuing and unmet challenge in the study of mononuclear transition metal systems is the presence of alternative relaxation pathways that short-circuit relaxation between the highest magnetic excited states, resulting in rapid relaxation at low temperatures and often in waist-restricted magnetic hysteresis.<sup>9,10</sup>

We sought to investigate the combination of these two separate design paradigms for transition metal single-molecule magnets and herein report the synthesis and characterization of  $[\text{Co}_4(\text{NP}^t\text{Bu}_3)_4][\text{B}(\text{C}_6\text{F}_5)_4]$  (**1**,  $^t\text{Bu}$  = *tert*-butyl, Figure 1), wherein a cluster of four low-coordinate cobalt centers are coupled via electronic communication. We find that the synergistic combination of these two effects results in a compound exhibiting both large magnetic anisotropy and the largest effective relaxation barrier to date for a transition metal cluster compound.

Compound **1** was isolated cleanly and in good yield as a dark green, air-sensitive crystalline solid from the one-electron oxidation of  $\text{Co}_4(\text{NP}^t\text{Bu}_3)_4$ ,<sup>11</sup> which features a square of four cobalt(I) centers each coordinated by two  $\mu^2$ -phosphinimidate ligands. Oxidation results in a structural distortion of the cluster that is most distinctly demonstrated by the decrease of the N–Co–N angles from an average value of  $178(1)^\circ$  for

Received: December 20, 2017

Published: January 23, 2018

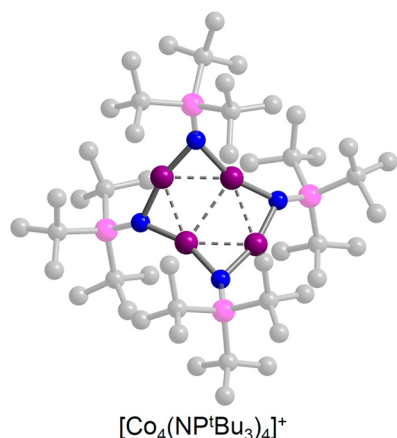


**Figure 1.** Crystal structure of the  $[\text{Co}_4(\text{NP}^t\text{Bu}_3)_4]^+$  cation in 1-2DFB. Violet, blue, pink, and gray spheres represent Co, N, P, and C atoms, respectively; H atoms, solvent molecules, the  $[\text{B}(\text{C}_6\text{F}_5)_4]^-$  counteranion, and disordered components are omitted for clarity. Selected distances (Å) and angles (deg) for the first disordered component: Co–N (avg) 1.872(19); Co...Co 2.3394(14), 2.3480(14), 2.3556(13), 2.3791(16); Co...Co (diagonal) 2.661(5), 3.887(5); N–Co–N (avg) 162(2).

$\text{Co}_4(\text{NP}^t\text{Bu}_3)_4$  to 162(2)° for **1**. The crystal structure of **1** reveals that the cationic cluster is disordered over two positions, although the two disordered components exhibit similar structural features (Table S2). The Co...Co distances in **1** are shorter than those found in  $\text{Co}_4(\text{NP}^t\text{Bu}_3)_4$  and range from 2.321(4) to 2.380(2) Å, values that are within the appropriate range for direct metal–metal interactions (Figure 1). The sum of the four Co–Co–Co angles is 360° within error, indicating that the four cobalt centers remain coplanar. It should be noted that, based on the Co–N bond distances, the diffraction data cannot be used to distinguish the oxidation state of each Co center.

The cyclic voltammogram of **1** in 1,2-difluorobenzene (DFB) exhibits the expected one-electron reversible  $[\text{Co}_4(\text{NP}^t\text{Bu}_3)_4]^{+/0}$  redox couple occurring at  $-2.44$  V vs  $[\text{Fc}/\text{Fc}^+]$ , as well as a one-electron reversible oxidation at  $-1.03$  V assigned to the  $[\text{Co}_4(\text{NP}^t\text{Bu}_3)_4]^{2+/+}$  couple (Figure S3). The large comproportionation constant of  $5.2 \times 10^{23}$  for the mixed-valence species  $[\text{Co}_4(\text{NP}^t\text{Bu}_3)_4]^+$  suggests a delocalized electronic structure for complex **1**, a consequence of direct orbital overlap through short Co...Co contacts. Similar electrochemical behavior was observed in hexanuclear  $[(^{\text{HL}})_2\text{Fe}_6(\text{L}')_m]^{n+}$  complexes possessing direct metal–metal orbital overlap.<sup>12</sup>

Variable-temperature dc magnetic susceptibility data collected on a microcrystalline solid sample of 1-2DFB at 1000 Oe reveal a  $\chi_M T$  product of 20.46 cm<sup>3</sup> K/mol at 300 K, a value that is much higher than the 4.875 cm<sup>3</sup> K/mol expected for three Co(I) centers and one Co(II) center that are magnetically isolated (Figure 2, red circles). This value corresponds to an  $S = 9/2$  ground state with  $g_{\text{iso}} = 2.57$ , suggesting complete delocalization of electrons via direct orbital overlap among the four Co centers. The result is consistent with the unpaired electrons residing in a single valence orbital manifold of a weak-field cluster.<sup>13</sup> Similarly,  $\text{Co}_4(\text{NP}^t\text{Bu}_3)_4 \cdot 2\text{THF}$  (THF = tetrahydrofuran) exhibits a well-isolated high spin ground state with a  $\chi_M T$  product of 10.68 cm<sup>3</sup> K/mol at 300 K, corresponding to an  $S = 4$  ground state with  $g_{\text{iso}} = 2.07$  (Figure 2, blue circles). With decreasing temperature, the  $\chi_M T$  product of  $\text{Co}_4(\text{NP}^t\text{Bu}_3)_4 \cdot 2\text{THF}$  decreases until a plateau at  $\sim 50$  K that is suggestive of a spin crossover transition, the details of which are under ongoing investigation. The downturn in  $\chi_M T$

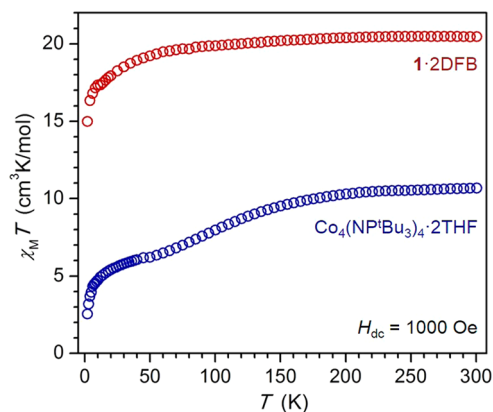


**Figure 2.** Variable-temperature molar magnetic susceptibility data for 1-2DFB and  $\text{Co}_4(\text{NP}^t\text{Bu}_3)_4 \cdot 2\text{THF}$  collected under an applied field of 1000 Oe.

below  $\sim 50$  K for  $\text{Co}_4(\text{NP}^t\text{Bu}_3)_4$  and below  $\sim 100$  K for **1** indicates the presence of magnetic anisotropy.

Variable-temperature, variable-field reduced magnetization data collected for 1-2DFB exhibit nonsuperimposable isofield lines, thus supporting the presence of magnetic anisotropy in the system (Figure S4). The data were fit to the following Hamiltonian

$$\hat{H} = D\hat{S}_z^2 + E(\hat{S}_x^2 - \hat{S}_y^2) + g\mu_B \mathbf{S} \cdot \mathbf{H} \quad (1)$$

where  $D$  and  $E$  are the axial and transverse zero-field splitting parameters, respectively,  $S_{x/y/z}$  is the electron spin projection onto the  $x/y/z$  axis,  $\mu_B$  is the Bohr magneton,  $g$  is the Landé  $g$ -factor, and  $\mathbf{H}$  is the magnetic field. The fit yields a surprisingly large negative  $D$  value of  $-12.34$  cm<sup>-1</sup>, with  $E = 3.49$  cm<sup>-1</sup>,  $g_{\parallel} = 2.48$ , and  $g_{\perp} = 2.82$ .

The relaxation dynamics of compound **1** were explored by carrying out ac magnetic susceptibility measurements on a powdered, microcrystalline sample of 1-2DFB in the presence of a 4-Oe ac field and zero dc field. The in-phase ( $\chi_M'$ ) and out-of-phase ( $\chi_M''$ ) susceptibility data were fit satisfactorily to a bimodal distribution by assuming the presence of two temperature-dependent relaxation processes with corresponding relaxation times  $\tau_1$  and  $\tau_2$  (see Equation S3 and Figure S9). We ascribe this behavior to the relaxation of the two disordered components observed in the crystal structure (see Supporting Information). In order to mitigate any crystal packing effects on the structural disorder, ac susceptibility data were also collected on a 10 mM frozen solution of 1-2DFB in the glassing solvent 2-methyltetrahydrofuran (2-MeTHF). For this sample,  $\chi_M''$  curves could be fit relatively well to a broad unimodal distribution ( $\alpha_{\text{average}} = 0.43$ ), which possibly suggested that **1** might exist as a distribution of conformations in solution (Figure 3a).

Slow relaxation in molecular systems occurs as a result of energy exchange between the crystal lattice and spin system via lattice vibrations known as phonons. When the magnitude of the energy exchanged is equivalent to a real excited state within a molecule, relaxation occurs via an Orbach process,<sup>14</sup> and the corresponding relaxation times exhibit an Arrhenius-type temperature dependence, as shown in the first term in eq 2. The zero-field Arrhenius plot for **1** measured in 2-MeTHF exhibits a significant divergence from linearity at low temperatures (Figure 3b, open circles). This curvature suggests that through-barrier relaxation processes are operative at these temperatures, as commonly observed for mononuclear sys-

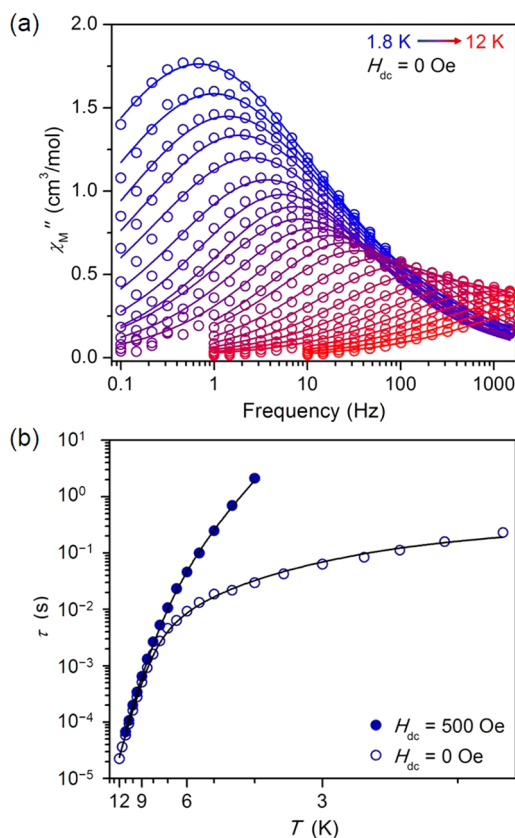


**Figure 3.** (a) Out-of-phase component of the magnetic susceptibility ( $\chi_M''$ ) for a sample of 1-2DFB prepared as a 10 mM solution in 2-MeTHF, collected under zero dc field. Solid lines represent fits to the data using the generalized Debye model. (b) Arrhenius plot of relaxation time  $\tau$  (log scale) versus  $T$  (inverse scale). Data collected under zero and 500 Oe applied dc fields are plotted as open and closed circles, respectively. Black lines represent the overall fit as described in the text.

tems.<sup>15</sup> Application of a small static field of 500 Oe results in a lengthening of the low-temperature relaxation times and suppression of this lower temperature relaxation process. In the corresponding Arrhenius plot, a linear regime at high temperatures overlaps with the zero-field data, suggesting that at these temperatures relaxation may favor an Orbach mechanism.

For the data collected under a 500-Oe applied field, the temperature dependence of the relaxation times was best fit using eq 2, with contributions from an Orbach mechanism and another spin–lattice process known as Raman relaxation, which occurs via virtual excited states and exhibits a power dependence on temperature:

$$\tau^{-1} = \tau_0^{-1} \exp\left(-\frac{U_{\text{eff}}}{k_B T}\right) + C_1 T^{n_1} \quad (2)$$

In this equation,  $\tau_0$  is a preexponential factor,  $U_{\text{eff}}$  is the effective spin reversal barrier,  $k_B$  is the Boltzmann constant,  $T$  is temperature,  $C_1$  is the Raman coefficient, and  $n_1$  is the Raman exponent.<sup>16</sup> It should be noted that relaxation through direct process was found to be negligible. Alternatively, for the zero applied field data, a satisfactory fit was found only when a second Raman process was introduced together with a quantum tunneling process,<sup>17</sup> as shown in eq 3.

$$\tau^{-1} = \tau_0^{-1} \exp\left(-\frac{U_{\text{eff}}}{k_B T}\right) + C_1 T^{n_1} + C_2 T^{n_2} + \tau_{\text{tunnel}}^{-1} \quad (3)$$

The 0- and 500-Oe data were simultaneously fit to the above equations while restraining  $U_{\text{eff}}$ ,  $C_1$ , and  $n_1$  to be the same across the two data sets in order to reduce parameter space. Raman exponents  $n_{1,2}$  were restrained to assume integer values. The best fitting results are listed in Table 1 and plotted in Figure S16.

**Table 1.** Parameters Used To Fit Temperature-Dependent Relaxation Times for 1-2DFB Extracted from AC Magnetic Susceptibility Measurements on a 10 mM Solution in 2-MeTHF

$H_{\text{dc}}$ (Oe)	0	500
$\tau_0$ (s)	$9.2 \times 10^{-10}$	$1.11 \times 10^{-9}$
$U_{\text{eff}}$ ( $\text{cm}^{-1}$ )	87	87
$C_1$ ( $\text{K}^{-n_1} \text{s}^{-1}$ )	$1.92 \times 10^{-6}$	$1.92 \times 10^{-6}$
$n_1$	9	9
$C_2$ ( $\text{K}^{-n_2} \text{s}^{-1}$ )	0.424	
$n_2$	3	
$\tau_{\text{tunnel}}$ (s)	0.37	

To the best of our knowledge, the spin reversal barrier of 87  $\text{cm}^{-1}$  determined from fitting is the highest among transition metal cluster single-molecule magnets,<sup>18</sup> exceeding the previous record barrier of 60  $\text{cm}^{-1}$  for  $\text{Mn}_6\text{O}_2(\text{Et-sao})_6(\text{O}_2\text{CR})_2(\text{EtOH})_6$ .<sup>8</sup> The barrier exhibited by **1** can be attributed to the large negative axial zero-field splitting parameter,  $D$ , although its value still falls short of the predicted magnitude, given the values of  $D$  and  $E$  extracted from fitting magnetization data and assuming that the spin relaxes via the highest molecular excited state. Indeed, with  $D = -12.34 \text{ cm}^{-1}$  and  $E = 3.49 \text{ cm}^{-1}$ , the total magnitude of the splitting within the ground  $S$  state of **1** is expected to be 292  $\text{cm}^{-1}$ . Alternatively, if relaxation occurs through the first excited states ( $M_S = \pm 7/2$ ), then the predicted  $U_{\text{eff}}$  value would be 93  $\text{cm}^{-1}$ , which closely matches the experimental value of 87  $\text{cm}^{-1}$ . Such relaxation behavior is reminiscent of many mononuclear single-molecule magnets, wherein magnetic relaxation occurs primarily through the first excited magnetic states instead of traversing the entire anisotropy barrier.<sup>19</sup>

The presence of Raman relaxation is another similarity between **1** and most mononuclear single-molecule magnets, and the Raman exponent of  $n_1 = 9$  is as expected for two-phonon relaxation of Kramers ions.<sup>16</sup> At zero field, a second phonon-mediated relaxation with  $n_2 = 3$  is present. This lower Raman exponent may arise from relaxation involving an optical acoustic two-phonon process, although more studies are required to draw a definitive conclusion (see Supporting Information).

Open, waist-restricted hysteresis loops were also observed for the solution sample of 1-2DFB below 3.6 K (Figure 4), and the absence of remnant magnetization agrees with the fast zero-field relaxation exhibited in the ac susceptibility data. Further comparison of variable-temperature field-cooled and zero-field-cooled magnetization data collected under a 1000-Oe dc field revealed a divergence at  $\sim 3$  K, indicating that it is around this temperature at which magnetic blocking occurs for **1** (Figure S14).

We have demonstrated that engineering strong electronic communication between low-coordinate metal centers provides an effective strategy for creating single-molecule magnets simultaneously exhibiting large spin and magnetic anisotropy.

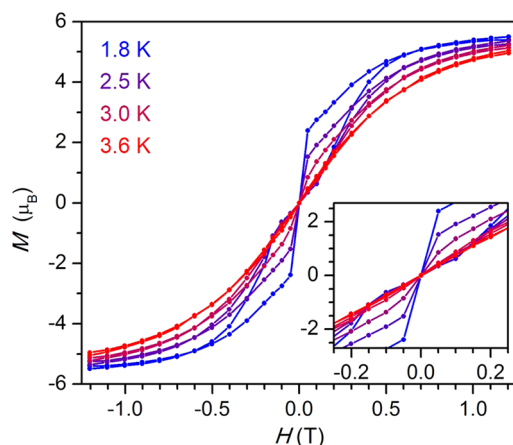


**Figure 4.** Variable-field magnetization data collected on a 10 mM solution of 1-2DFB in 2-MeTHF at an average field sweep rate of 30 Oe/s. Solid lines are guides for the eye. Inset shows a magnified view of the plots near the origin.

Indeed, in spite of contributions from through-barrier processes such as Raman relaxation, relaxation at high temperatures in **1** appears to favor an Orbach mechanism proceeding via the first magnetic excited states. This relaxation likely arises from the total spin of the cluster, and although relaxation does not proceed through the highest excited  $M_S$  states, the corresponding effective relaxation barrier is the largest to date for a transition metal cluster. Ongoing studies will seek to identify systems wherein anisotropy and spin may be further enhanced to favor Orbach relaxation via the highest excited states.

## ■ ASSOCIATED CONTENT

### Supporting Information

The Supporting Information is available free of charge on the ACS Publications website at DOI: 10.1021/jacs.7b13394.

Full experimental details, crystallographic, and additional magnetic data (PDF)

Data for  $C_{48}H_{108}Co_4N_4P_4$ ,  $BC_{24}F_{20}$ ,  $1.61(C_6H_4F_2)$  (CIF)

## ■ AUTHOR INFORMATION

### Corresponding Author

\*jrlong@berkeley.edu

### ORCID

Khetpakorn Chakarawet: 0000-0001-5905-3578

Jeffrey R. Long: 0000-0002-5324-1321

### Notes

The authors declare no competing financial interest.

## ■ ACKNOWLEDGMENTS

This work was funded by NSF Grant CHE-1464841. We thank the government of Thailand for support of K.C. through a Development and Promotion of Science and Technology (DPST) scholarship. Single-crystal X-ray diffraction data were collected on Beamline 11.3.1 at the Advanced Light Source, which is supported by the Director, Office of Science, Office of Basic Energy Sciences, of the U.S. Department of Energy under Contract no. DE-AC-02-05CH11231. We additionally thank Dr. Rodolphe Clérac for valuable discussions, Lucy E. Darago for assistance with the paper revision, and Dr. Katie R. Meihaus for editorial assistance.

## ■ REFERENCES

- (a) Sessoli, R.; Tsai, H.-L.; Schake, A. R.; Wang, S.; Vincent, J. B.; Foltling, K.; Gatteschi, D.; Christou, G.; Hendrickson, D. N. *J. Am. Chem. Soc.* **1993**, *115*, 1804. (b) Sessoli, R.; Gatteschi, D.; Caneschi, A.; Novak, M. A. *Nature* **1993**, *365*, 141.
- Mannini, M.; Pineider, F.; Sainctavit, P.; Danieli, C.; Otero, E.; Sciancalepore, C.; Talarico, A. M.; Arrio, M.; Cornia, A.; Gatteschi, D.; Sessoli, R. *Nat. Mater.* **2009**, *8*, 194.
- Leuenberger, M. N.; Loss, D. *Nature* **2001**, *410*, 789.
- Bogani, L.; Wernsdorfer, W. *Nat. Mater.* **2008**, *7*, 179.
- (a) Rinehart, J. D.; Long, J. R. *Chem. Sci.* **2011**, *2*, 2078. (b) Guo, F.-S.; Day, B. M.; Chen, Y.-C.; Tong, M.-L.; Mansikkamäki, A.; Layfield, R. A. *Angew. Chem., Int. Ed.* **2017**, *56*, 11445. (c) Goodwin, C. A. P.; Ortu, F.; Reta, D.; Chilton, N. F.; Mills, D. P. *Nature* **2017**, *548*, 439.
- Gatteschi, D.; Sessoli, R.; Villain, J. *Molecular Nanomagnets*; Oxford Univ. Press, 2006.
- (a) Ruiz, E.; Cirera, J.; Cano, J.; Alvarez, S.; Loose, C.; Kortus, J. *Chem. Commun.* **2008**, *2*, 52. (b) Neese, F.; Pantazis, D. A. *Faraday Discuss.* **2011**, *148*, 229.
- Milios, C. J.; Vinslava, A.; Wernsdorfer, W.; Moggach, S.; Parsons, S.; Perlepes, S. P.; Christou, G.; Brechin, E. K. *J. Am. Chem. Soc.* **2007**, *129*, 2754.
- Yao, X.-N.; Du, J.-Z.; Zhang, Y.-Q.; Leng, X.-B.; Yang, M.-W.; Jiang, S.-D.; Wang, Z.-X.; Ouyang, Z.-W.; Deng, L.; Wang, B.-W.; Gao, S. *J. Am. Chem. Soc.* **2017**, *139*, 373.
- (a) Zadrozny, J. M.; Xiao, D. J.; Atanasov, M.; Long, G. J.; Grandjean, F.; Neese, F.; Long, J. R. *Nat. Chem.* **2013**, *5*, 577. (b) Carl, E.; Demeshko, S.; Meyer, F.; Stalke, D. *Chem. - Eur. J.* **2015**, *21*, 10109. (c) Rechkemmer, Y.; Breitgoff, F. D.; van der Meer, M.; Atanasov, M.; Haki, M.; Orlita, M.; Neugebauer, P.; Neese, F.; Sarkar, B.; van Slageren, J. *Nat. Commun.* **2016**, *7*, 10467.
- Camacho-Bunquin, J.; Ferguson, M. J.; Stryker, J. M. *J. Am. Chem. Soc.* **2013**, *135*, 5537.
- Hernández Sánchez, R.; Zheng, S.-L.; Betley, T. A. *J. Am. Chem. Soc.* **2015**, *137*, 11126.
- (a) Cotton, F. A.; Daniels, L. M.; Matonic, J. H.; Murillo, C. A. *Inorg. Chim. Acta* **1997**, *256*, 277. (b) Hernández Sánchez, R.; Betley, T. A. *J. Am. Chem. Soc.* **2015**, *137*, 13949.
- Orbach, R. *Proc. R. Soc. London, Ser. A* **1961**, *264*, 458.
- See for example: Zadrozny, J. M.; Atanasov, M.; Bryan, A. M.; Lin, C. Y.; Rekker, B. D.; Power, P. P.; Neese, F.; Long, J. R. *Chem. Sci.* **2013**, *4*, 125.
- Shrivastava, K. N. *Phys. Status Solidi B* **1983**, *117*, 437.
- Gatteschi, D.; Sessoli, R. *Angew. Chem., Int. Ed.* **2003**, *42*, 268.
- The statement does not take into account the work on dinuclear  $Co(hfipip)_2$  complexes due to an inconclusive structure-magnetic property relationship: Yoshihara, D.; Karasawa, S.; Koga, N. *Polyhedron* **2011**, *30*, 3211.
- (a) Harman, W. H.; Harris, T. D.; Freedman, D. E.; Fong, H.; Chang, A.; Rinehart, J. D.; Ozarowski, A.; Sougrati, M. T.; Grandjean, F.; Long, G. J.; Long, J. R.; Chang, C. J. *J. Am. Chem. Soc.* **2010**, *132*, 18115. (b) Zadrozny, J. M.; Xiao, D. J.; Long, J. R.; Atanasov, M.; Neese, F.; Grandjean, F.; Long, G. J. *Inorg. Chem.* **2013**, *52*, 13123.